Comparison of a Portable Field Spectrometer and Automated Imaging on Geothermal Drill Core: A Pilot Study

Kurt Kraal[1], Bridget Ayling[1], Wendy Calvin[2], and Dave Browning[3]

[1] Great Basin Center for Geothermal Energy, University of Nevada Reno

[2]Dept. of Geological Sciences and Engineering, University of Nevada Reno

[3]TerraCore

Keywords

Hyperspectral, Mineral alteration, Infrared spectroscopy, Drill core, EGS, Fallon FORGE, ASD

ABSTRACT

Infrared reflectance spectroscopy is effective at identifying hydrothermal alteration mineralogy, which can provide information about past temperatures and fluid flow pathways that are important for geothermal exploration and assessment. Advances in hyperspectral imaging technology allow for rapid analyses and the creation of high-resolution mineral maps of geothermal drill core. We performed a pilot study on core from the Fallon FORGE EGS site (Well FOH-2) to compare portable Analytical Spectral Devices (ASD) spectral measurements with automated high-resolution imaging spectroscopy. This study focuses on Well FOH-2's Tertiary volcanic section consisting of Miocene basaltic andesite. First, we used an ASD FieldSpec Pro portable spectroradiometer that collects spectra in the VNIR/SWIR range (400 nm to 2500 nm) to collect 67 spectral measurements at approximately five-inch intervals from about 35 feet of core from four depth ranges between 2834 and 4005 feet targeting both zones of alteration and unaltered rock. Spectral data at each sampling point obtained by the ASD represent mixtures of minerals located within the instrument's 20mm diameter field of view. We compared this data with spectral maps acquired using a TerraCore Hyperspectral Core Imaging System (HCIS), with a pixel size of 1.2mm, equipped with FENIX VNIR-SWIR and OWL LWIR (8-12μm) cameras, as well as an RGB camera to create a high resolution (0.12 mm pixel size) image of the same drill core. We show that both methods are effective in identifying the dominant alteration mineralogy within the drill core, but the spectral mapping capabilities of the HCIS provide greater opportunity to evaluate spatial relationships of alteration minerals across a continuous dataset.

1. Introduction

Infrared reflectance spectroscopy is an effective tool to rapidly collect mineralogical data, especially alteration mineralogy that is difficult to distinguish in hand sample or by petrographic methods. The technique does not require the lengthy sample preparation required for X-Ray Diffraction (XRD) analysis (Calvin and Pace 2016, Thompson 1999). This method is effective because most rock forming minerals have diagnostic absorption features in either the Visible Near- and Short-Wave Infrared (VNIR/SWIR, 400-2500 nm) or the Long Wave Infrared (LWIR, 8-12μm) (Clark 1999). Applied to geothermal drill core, this method allows for the identification of alteration phases (Calvin and Pace 2016, Yang et al. 2000, 2001), useful for exploration and reservoir assessment in analyzing past temperatures, past fluid flow pathways, fluid acidity, and rock properties such as permeability, porosity, and strength (Browne 1978, Reyes 1990, Wyering et al. 2014, Frolova et al. 2013). Hyperspectral methods can also be applied to Enhanced or Engineered Geothermal Systems (EGS) that require extensive sub-surface characterization. Advances in high-resolution automated imaging spectroscopy are now capable of collecting a spatially continuous hyperspectral data set from drill core that provides a new opportunity to evaluate spatial relationships of alteration minerals. This pilot study compares new advances in imaging spectroscopy, collected by the TerraCore Hyperspectral Core Imaging System (HCIS), with a portable Analytical Spectral Devices (ASD) FieldSpec Pro, the more common technology, using geothermal drill core from the Fallon EGS site.

2. Background

2.1 High-Spatial Resolution SWIR Spectroscopy for Geothermal

Infrared absorption spectroscopy is of particular interest for geologic materials because many rock forming minerals display absorption features when interacting with electromagnetic radiation in the VNIR-SWIR and LWIR wavelength ranges (Geiger 2004). Absorption features in this range are caused by either electronic processes, dependent on unfilled d orbitals, or vibrational processes, dependent on bonds in a crystal lattice. Molecules that show absorption features in the SWIR are O-H, C-O, cation-OH (Clark 1999). The VNIR-SWIR regions were deemed suitable for this study based on their ability to map amphiboles, and phyllosilicates, including mica, chlorite, and smectites (Figure 1). However, because absorption bands for Si-O are not found in the SWIR range, SWIR is not useful for identifying all silicates (Figure 1). Spectral libraries, such as the U.S. Geological Survey spectral library are compared with collected spectra in order to identify minerals (Clark et al. 1990). In addition to mineral identification, absorption bands are sensitive to crystal structure and subtle changes in chemistry (Clark 1999). The relative intensity of absorption bands can also be correlated to mineral abundance, where stronger absorption bands are related to higher abundance (or more pervasive alteration).

Common minerals found in geothermal systems with SWIR responsive features include: aluminum phyllosilicates, such as smectites; the kaolinite group; the illite group; Fe-Mg phyllosilicates, such as chlorite group minerals; epidote group minerals; carbonate; and zeolites

(Browne 1978, Calvin and Pace 2016, Figure 1). Mapping of alteration in drill core was shown to be effective in fossil hydrothermal systems by Thompson et al. (1998), where mineral assemblages identified aid in multiple types of ore deposit interpretation. Yang et al. (2000, 2001) investigated core from the Wairakei and Broadlands-Ohaaki geothermal fields using a portable SWIR spectrometer and characterized the alteration mineralogy and the zoning of alteration minerals. Calvin and Pace (2016) conducted a pilot study using a portable SWIR spectrometer on geothermal drill core, and identified alteration minerals and their zonation from point spectra measurements.

	Structure	Group	Example	VNIR Response	SWIR Response	LWIR Response
Silicates	Inosilicates	Amphibole	Actinolite	Non-diagnostic	Good	Good
		Pyroxene	Diopside	Good	Moderate	Good
	Cyclosilicates	Tourmaline	Dravite	Non-diagnostic	Good	Moderate
	Nesosilicates	Garnet	Andradite	Moderate	Non-diagnostic	Good
		Olivine	Forsterite	Good	Non-diagnostic	Good
		Zircon	Zircon	Good	Non-diagnostic	Non-diagnostic
	Sorosilicates	Epidote	Clinozoisite	Non-diagnostic	Good	Good
	Phyllosilicates	Mica	Muscovite	Non-diagnostic	Good	Moderate
		Chlorite	Clinochlore	Non-diagnostic	Good	Moderate
		Clay Minerals	Kaolinite	Non-diagnostic	Good	Moderate
			Illite	Non-diagnostic	Good	Moderate
	Tectosilicates	Feldspar	Orthoclase	Non-diagnostic	Non-diagnostic	Good
			Albite	Non-diagnostic	Non-diagnostic	Good
		Silica	Quartz	Non-diagnostic	Non-diagnostic	Good
Non-Silicates	Carbonates	Calcite		Non-diagnostic	Good	Good
		Dolomite		Non-diagnostic	Good	Good
	Hydroxides	Gibbsite		Non-diagnostic	Good	Moderate
	Sulphates	Alunite	Alunite	Non-diagnostic	Good	Moderate
			Barite	Non-diagnostic	Non-diagnostic	Good
	Borates		Borax	Non-diagnostic	Good	Uncertain
	Halides	Chlorides	Halite	Non-diagnostic	Moderate	Uncertain
	Phosphates	Apatite	Apatite	Moderate	Moderate	Good
			Amblygonite	Moderate	Good	Good
	Hydrocarbons		Bitumen	Non-diagnostic	Good	Uncertain
	Oxides		Hematite	Good	Non-diagnostic	Non-diagnostic
		Spinel	Magnetite	Non-diagnostic	Non-diagnostic	Non-diagnostic
	Sulphides		Pyrite	Non-diagnostic	Non-diagnostic	Non-diagnostic

Figure 1: Common minerals that are spectrally-responsive in visible-near, short-wave, and long-wave infrared by hyperspectral scanning.

Automated hyperspectral core imaging is a new development for logging mineralogy in core. In addition to being automated, spectral datasets can be continuous across many meters of core and higher resolution (1mm pixel size or less) can give spatial context to observed spectra. Automated core imaging SWIR spectroscopy has been used to map alteration in core from ore deposits (Huntington et al. 2006, Tappert et al. 2011, Kokaly et al. 2017, Zhou et al. 2017), and for hydrocarbon exploration (Ayling et al. 2016, Mehmani et al. 2017), however no published

studies show its applications to geothermal core. Zhou et al. (2017) compares ASD to high spatial resolution core scanning at a high sulfidation gold deposit, a porphyry deposit, and a Carlin deposit and found that the core scanning located zones of alteration and alteration mineralogy that was missed by the portable ASD, as well as leading to new interpretations of alteration patterns with implications for targeting ore at the regional scale.

2.2 Geologic Background of Fallon EGS Case Study

The Fallon Forge EGS site is located in the Carson Sink, Churchill County, Nevada, and is being evaluated as a test site for the Frontier Observatory for Research in Geothermal Energy (FORGE). A detailed geologic characterization of the Fallon Forge site was provided by Siler et al. (2018). Fallon was the site of previous geothermal exploration because of high heat flow, however its low permeability impedes the development of an active hydrothermal system, and thus is a candidate for EGS rather than as a conventional geothermal. The lithology at the FORGE site is basin Quaternary to Miocene sedimentary fill, Tertiary volcanics primarily of Miocene mafic to mafic-intermediate composition, and a mixed composition metamorphic Mesozoic basement composed of Triassic to Jurassic medium-low grade metasedimentary and metavolcanics rocks, with Jurassic-Cretaceous granitic intrusions. Previous XRD work performed on cuttings from seven wells (FOH-3, 82-35, 61-36, 84-31, 88-24, FDU-2D, and 18-5) to characterize the alteration found argillic, phyllic, and propylitic alteration zones representing temperatures higher than currently measured in the wells. It was suggested that this zonation was a product of a past hydrothermal system that is no longer active (Jones and Moore 2013). The drill core used in this study is from well FOH-2, which contains quaternary sediments, and the Tertiary volcanic section composed primarily of Miocene vesicular basaltic-andesite, and no XRD work has been completed on this core previously. The core used in this study came from 3 intervals, 2834-2842 ft (863-866 m), 3247-3255 ft (990-993 m), and 3946-3955 ft (1203-1206 m), all within the Tertiary volcanic section of basaltic andesite.

3. Methods

3.1 ASD

For this study, we utilized an ASD FieldSpec Pro portable spectroradiometer that measures in the VNIR/SWIR range to collect 67 spectra at approximately five-inch intervals from about 35 feet of core in four core boxes for the intervals noted previously. The data collection targeted both zones of alteration and unaltered rock. Spectral data at each sampling point obtained by the ASD represent mixtures of minerals located within the instrument's 20mm diameter field of view. The data collection calibrates the observation relative to a halon plate so that the resulting measurement is one of calibrated reflectance that can be directly compared to library spectra for mineral identification using software packages such as the Environment for Visualizing Images (ENVI).

3.2 Hyperspectral Core Imaging System

The TerraCore^{TM} imaging system (HCIS) used in this study operates via stationary line-scanning cameras, where the core box is placed on a table that is passed underneath the cameras at a

controlled rate. This method allows for imaging the entire core box, with an average image collection speed of approximately 90 seconds. During each scan, a white and dark reference is collected for image calibration. The HCIS utilizes 411 bands covering the VNIR-SWIR (463 nm – 2476 nm) with sampling approximately every 5 nm. The FENIX VNIR-SWIR spectral camera has a pixel size of 1.2mm. In addition to a hyperspectral image, an RGB camera creates a high resolution (0.12 mm pixel size) image of the same drill core simultaneously.

The spectral data are converted to reflectance and the extraneous material such as the core box are masked to avoid mixed spectra from interfering with mineral identification. Products created throughout the various stages of testing range from mineral maps demonstrating mineralogical variance, to feature extractions of numerical data. Feature extractions are tracked by measuring the depth, or strength, and location of specific absorption features. This data is processed and displayed in TerraCore's Intellicore software.

4. Results

4.1 Minerals Identified with SWIR

Both the ASD and the HCIS identified 3 alteration endmember phases: calcite, saponite, and an unknown mineral or mineral combination likely mixed montmorillonite with Fe-smectites or Fe-chlorite like chamosite (Figure 2). Calcite is identified in two core boxes, and by all methods described (Figure 2a). Saponite is identified by its asymmetric 1.4 μm and 1.9 μm absorption features and 2.31 μm absorption feature (Figure 2b). The unknown clay mixture is only found in the second depth interval and does not match any known library minerals (Figure 2c). Its spectrum contains an absorption doublet located at 2.21 μm and 2.25 μm that suggests that it is a mixture with a mineral containing an Al-OH bond, suggested by the 2.21 μm feature, and an Fe-OH bond, like in Fe-smectite varieties, chamosite, and other iron bearing phyllosilicates, however it lacks any absorption features beyond 2.25 μm and therefore does not directly match with library spectra for any chlorite varieties. These absorption bands are not found separate in any of our data and therefore we assume that if it is a mineral mixture, that these minerals are intimately mixed. Although we were not able to identify the exact mineral or mineral combination of the 'mystery' phase mapped, further XRD or petrographic work may identify it, providing new insight.

4.2 Method Comparison using ROIs

To compare the point spectra collected from ASD, and the high spatial resolution spectra from the HCIS, we collected mean spectra from the image within each ASD measurement's field of view using ENVI's Region Of Interest (ROI) tool. The mean spectra represents the average of the spectra within the ROI, and we assume that this is similar to the way the ASD creates an average spectra from the different minerals within its field of view. In most cases, the spectra collected from the ASD and the ROI mean spectra from the HCIS image match (examples shown in Figures 2 and 3). The few locations where they do not match may be related to inaccurate ROI location rather than differences between the instruments.

The high resolution hyperspectral images created by the HCIS allows for analysis of spatial relationships of minerals due to smaller pixel size, compared to the ASD's 20mm field of view. Figure 3 also shows a transect across the ASD's 20mm field of view, as well as associated spectra and the ROI mean from the HCIS data. Notice the variability within the field of view that is lost and displayed as a mixture by the ASD due to the larger field of view, compared to the variability within at higher resolution. Within the ASD's field of view there is relatively weak clay alteration surrounding a filled vesicle with a saponite rim and weakly altered mystery mineral center, all information that would be missed if reliant on the ASD measurement alone.

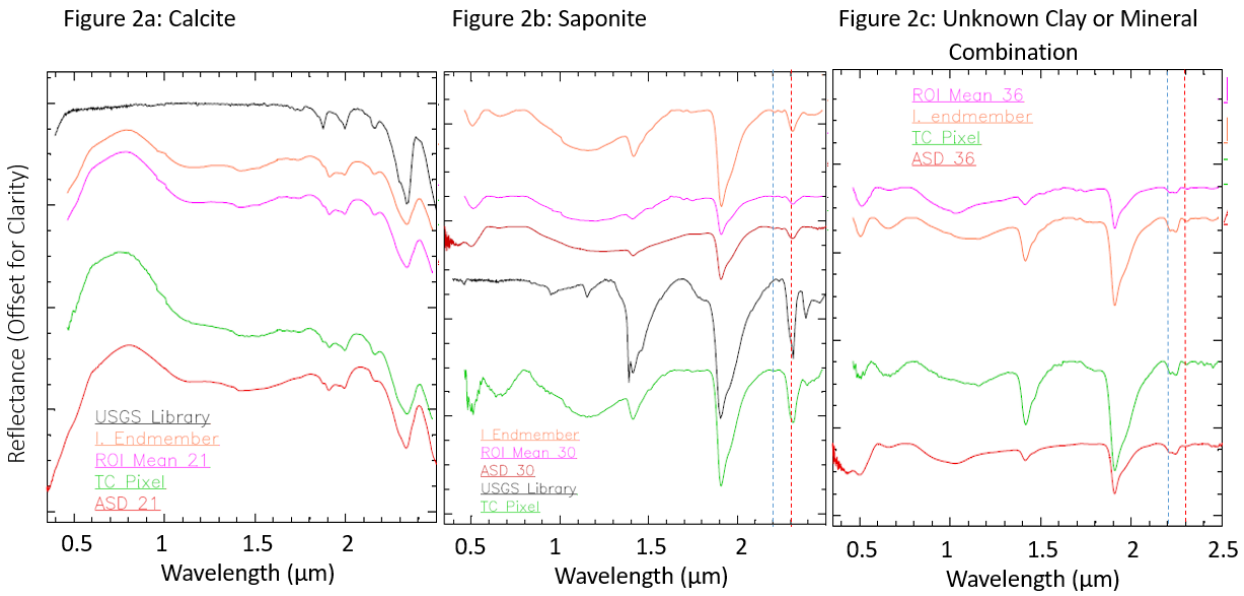

Figure 2: Example Core Spectra for (a) calcite, (b) saponite, (c) 'mystery' mineral detected in this study. In each panel, the black line is well-characterized pure minerals from the USGS standards database (Clark et al. 1990), red lines are ASD spectra, green lines are individual spectral pixels from the HCIS data, magenta lines are mean spectra from ROIs in the HCIS data (see text for details), and orange lines are Intellicore endmember spectra (see Figure 4 and text). These spectra are representative of single minerals, but many core spectra show variations in relative strength in features, and mineral mixtures. The dashed blue line is at 2.2 µm, and the dashed red line is 2.3 µm, the approximate location of the Al-OH and Fe-OH band respectively. Figures 2b and 2c show continuum removed spectra to aid in identification of absorption features.

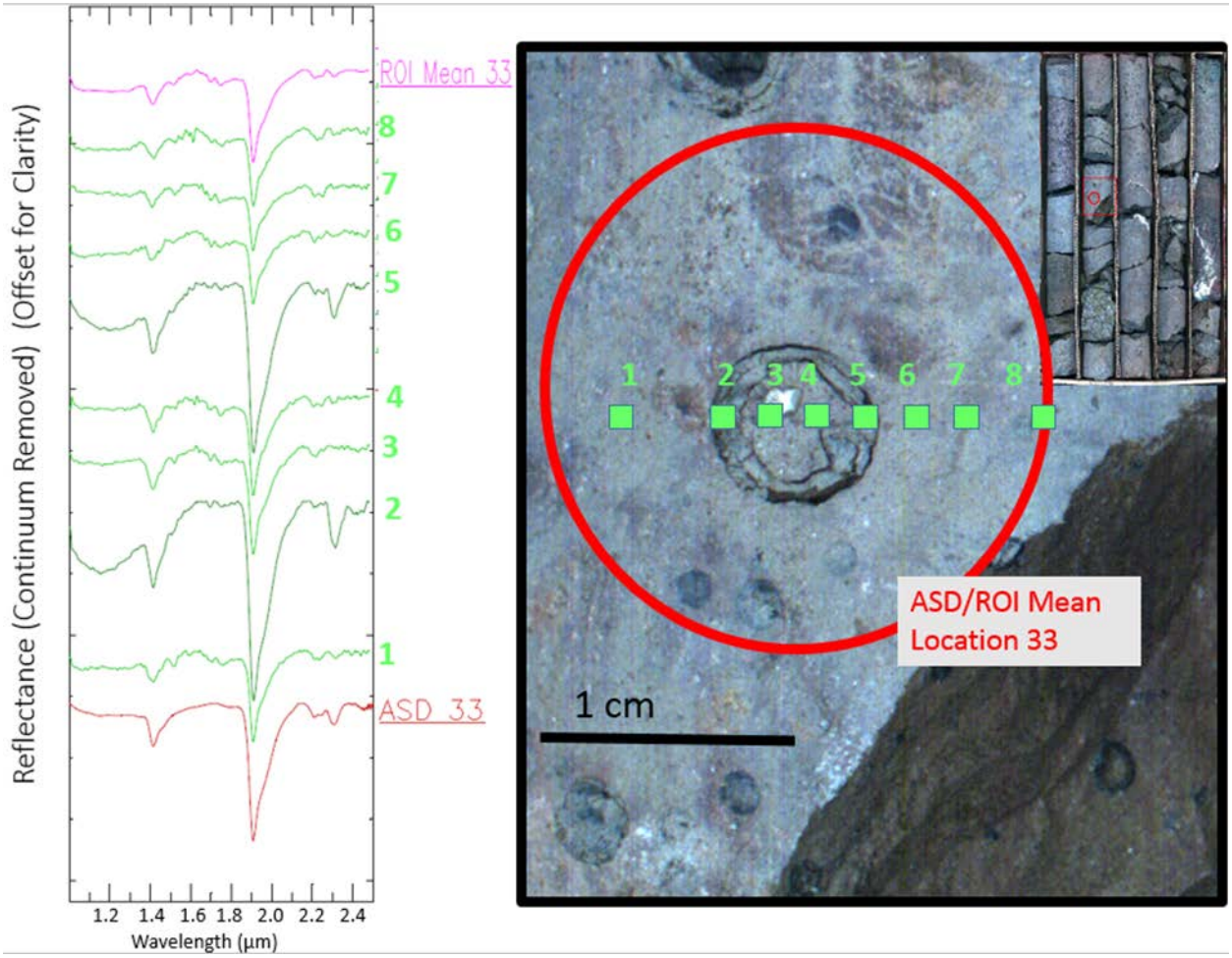

Figure 3: Comparison between ASD measured spectra, Region of Interest mean spectra for the same location collected by HCIS, and a HCIS pixel transect across the region to demonstrate the variability within. The red circle represents the location of the ASD measurement and the Region Of Interest. The red spectra is the ASD measurement, the magenta spectra is the ROI mean for the same region, and the green spectra correspond to the HCIS data found at the green pixels in the image on the right (pixels not to exact scale). Note the Dark green spectra (2, 5) and their location on the rims of the altered vug. See text for discussion.

4.3 Spectral Mapping Investigations

The data collected by the HCIS allows for mineral mapping techniques similar to those done in remote sensing data processing. TerraCore's Intellicore program can produce mineral maps such as the one shown in Figure 4, based on automated spectral endmember identification and further analysis by an expert spectroscopist (Example Intellicore Endmembers shown in Figure 2). To compare, an image of the core box is shown to the right with ASD sampling locations marked, as well as the corresponding ASD spectra, and what the spectra are identified as based on individual analysis. Figure 4 shows that much of the spatial relationships between alteration minerals are lost at lower resolution despite similar minerals being observed. Furthermore, the ASD also tends to see mineral mixtures more often than the HCIS, although mineral mixtures are still

prevalent in the HCIS mineral map. Note that for this pilot study, the ASD sampling density within the core box is higher than might be done for multiple kilometers of core.

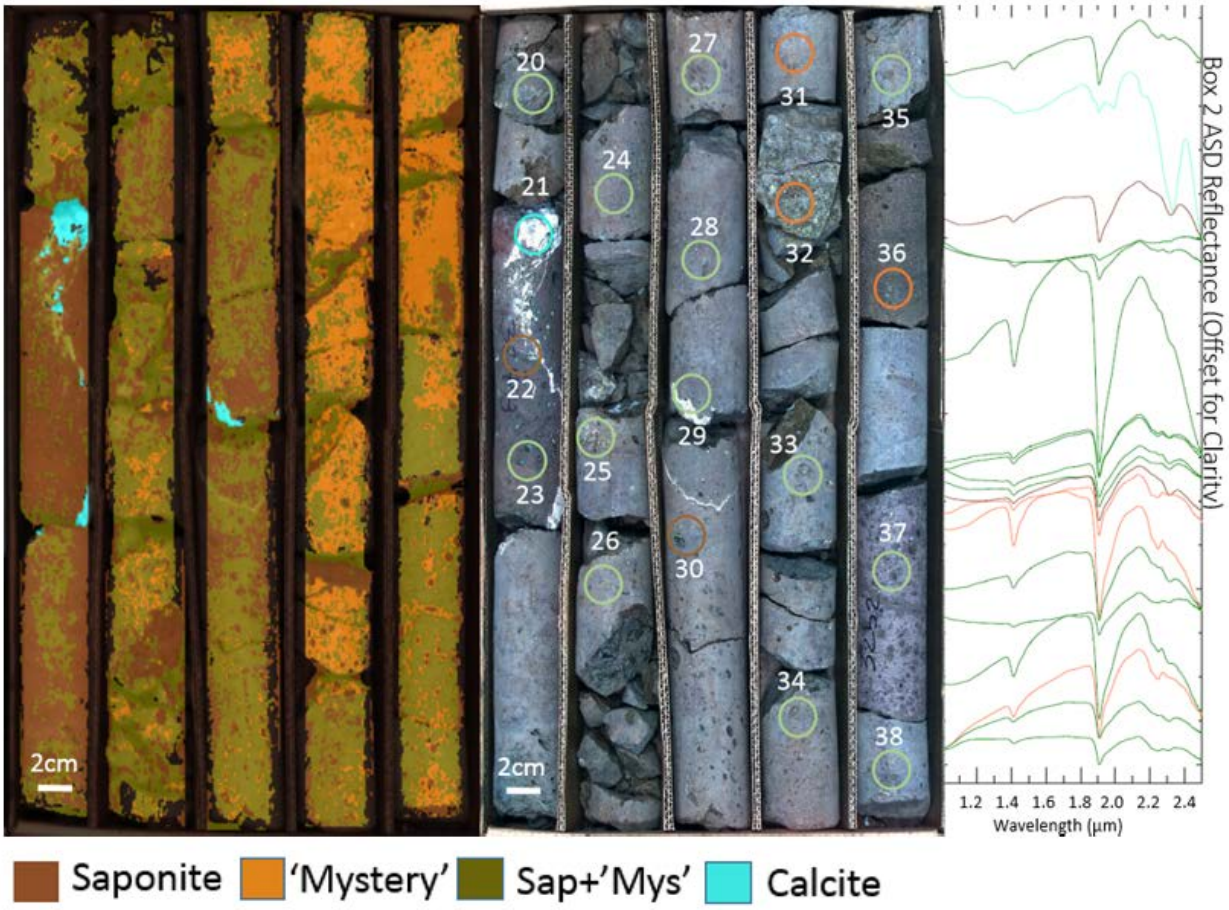

Figure 4: Well FOH-2, Box 2, 959-961 m (3147-3153 ft). Left: Mineral Map created in Intellicore. Light blue represents pure calcite (Figure 2a), dark blue dominantly saponite (Figure 2b), orange dominantly mystery mineral (Figure 2c), and green showing areas where the saponite/mystery mineral are approximately equal based on 2200 nm and 2300 nm feature strength (See Figure 3 ASD 33 for example). Black represents unidentified spectra (due to not being core or having no recognizable absorption features). Middle: RGB image of core, circles represent ASD measurement locations, labeled by order measured. Color represents minerals identified. Right: Corresponding spectra from the ASD, in order from top (20) to bottom (38) in this box.

One example of an additional spectral mapping technique is shown in Figure 5, a map of "alteration intensity" assuming the depth of the 1.9 μm absorption feature, associated with an Al-OH bond, corresponds to abundance of clays. This method will not capture carbonates, however, as we see in Figure 4, carbonates only occur in a few locations. In Figure 5, the areas with the deepest feature depth and highest alteration, are located within the vugs, veins, and on open fracture faces, while most other areas of the core are relatively less altered.

5. Discussion

The high-spatial resolution hyperspectral imaging creates new ways to investigate geothermal drill core and to get the most out of drilling core. Saponite dominates the alteration of core from intervals 2834-2842 ft (863-866 m), 3247-3255 ft (990-993 m), and 3946-3955 ft (1203-1206 m), and is most abundant in vugs and in veins, although it is present as an alteration phase even in areas without obvious alteration. The mystery mineral is most prevalent in the center box 3247-3255 ft (990-993 m), particularly on fractured faces, and in vugs and distributed throughout much of the core at this interval, while being mostly absent in the other core intervals. Carbonate is found in veins of the first two intervals, but not in the deepest interval.

Saponite is a common mineral in geothermal systems. Saponite is also associated with calcite and aragonite as scale in the Dixie Valley geothermal system, and as scale in geothermal wells from the Kyusy geothermal system in Japan (Hulen et al. 1999, Yagi et al. 2000). It has been found as the primary phyllosilicate associated with the permeable zone at temperatures above 200 ^{o}C in the Pantelleria caldera geothermal system (Fulignati et al. 1997), and is considered a metastable phase in high fracture permeability geothermal systems of Chipilapa (Patrier 1996).Saponite is found with montmorillonite as an argillic alteration feature acting as a “cap rock” at Medicine Lake, California (Hulen and Lutz 1999). At Medicine Lake, saponite is associated with the more mafic volcanic units compared to montmorillonite. Its thermal stability p to ~300 ^{o}C (Eberl et al. 1978), compared to montmorillonite which is stable to 180 ^{o}C (Hulen and Lutz 1999, Reyes 1990). Hulen and Lutz (1999) also point out the great ability of saponite to impede permeability in a hydrothermal system due to its high thermal stability and its mechanical behavior that allows it to flex instead of break when stressed. This may add to the low permeability found at the Fallon site, where saponite-montmorillonite smectites fill fractures and voids and impede fluid flow, although a survey of deeper core might provide more insight on mineralogical effects on the permeability at depth.

The unknown mineral or mineral mixture may represent a mixture between montmorillonite and Fe-smectites or montmorillonite and Fe-rich Mg-poor chlorite like chamosite. The combination of montmorillonite and chlorite is commonly found in geothermal systems at the transition between smectite dominated zones to higher temperature chlorite dominant zones. This is interpreted to be diagnostic of temperatures between 180-220 ^{o}C (Henley and Ellis 1983). The fact that this mineral is observed in the intermediate depth box but not in the other boxes suggests that there is something different at this depth interval: perhaps the host rock has a different composition, or this interval is near a past fluid-flow pathway, or these spectra may reflect rock that is less altered and in a transition state between the primary mineralogy of iron-bearing silicates such as pyroxenes and amphiboles altering to saponite, the most abundant iron-bearing phyllosilicate in this core.

6. Conclusion

SWIR was effective in identifying and mapping the distribution of alteration in drill core from the Fallon FORGE EGS site, although additional work may be required to identify the unknown clay or clay mixture mineral. Comparisons between ASD and HCIS methods shows that both can

be effectively employed for alteration mapping, however the HCIS's ability to construct hyperspectral images of drill core has the potential for evaluation of spatial relationships of alteration minerals, as well as a greater chance to observe pure mineral spectra than mixed mineral spectra, therefore higher accuracy mineral identification. The smectite alteration observed at the Fallon FORGE site for these depth intervals conforms to previously acquired data from adjacent holes within the area, however this study provides new context to the spatial relationships of the alteration phases in the drill core of the tertiary volcanic sequence, and more detail about smectite varieties lumped previously as "smectites".

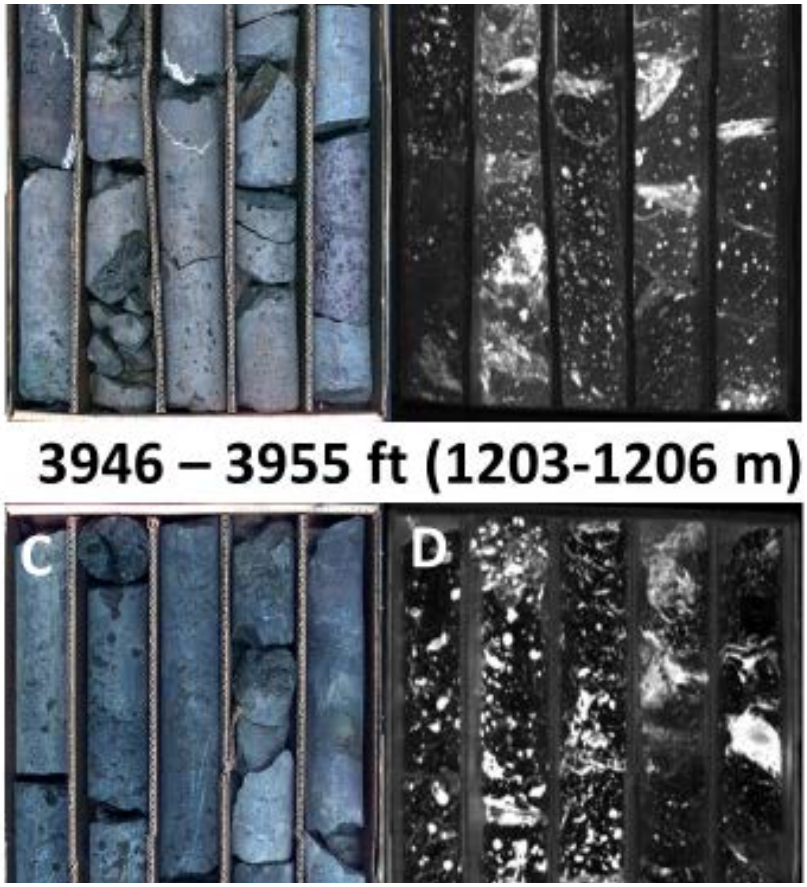

Figure 5: Alteration intensity maps with corresponding RGB core images. Image A and B are from Box 2 (3247-3255 ft), and C and D are from box 3 (3946-3952 ft). Light areas represent areas of high alteration, based on the continuum removed feature depth of the 1.9 µm absorption feature, associated with Al-OH bonds in clays. Dark areas represent areas of low alteration or clay content, and shallow 1.9 µm feature depth.

For future work we plan to image more geothermal drill core using HCIS technology across larger depth intervals to develop a greater understanding of the changes in alteration across the core. We also plan to incorporate LWIR imaging to identify non-hydrated silicate minerals without diagnostic features in the SWIR. We are also currently processing additional data from the Fallon FORGE site from sidewall cores collected from the metamorphic basement from recent drilling of the Phase 2B test well (Well 21-31). In addition to further investigations of the

Fallon FORGE site, we plan to apply this technique to geothermal drill core and cuttings from conventional active hydrothermal systems to characterize alteration zoning and mineral spatial relationships in order to assess of past temperatures, fluid flow pathways, and relate alteration to rock physical properties, such as strength, permeability, and porosity, and the types of alteration to rock electrical properties, useful in most pre-drilling geothermal exploration. We also plan to compare our hyperspectral datasets to petrographic and XRD methods for additional validation of the methodology. We anticipate that the application of this method to the geothermal systems of the Great Basin region will lead to new understandings of their geochemical and geomechanical behavior.

REFERENCES

Ayling, B., Huntington, J., Smith, B., Edwards, D., (2016), Hyperspectral logging of middle Cambrian marine sediments with hydrocarbon prospectivity: a case study from the southern Georgina Basin, northern Australia. Australian Journal of Earth Sciences, v. 63(8), p. 1069–1085.

Browne, P. R. L. (1978). Hydrothermal alteration in active geothermal fields. Annual review of earth and planetary sciences, 6(1), 229-248.

Calvin, W. M., & Pace, E. L. (2016). Mapping alteration in geothermal drill core using a field portable spectroradiometer. Geothermics, 61, 12-23.

Clark, R.N. (1999) Spectroscopy and Principles of Spectroscopy. Ch. 1 in Remote Sensing for the Earth Sciences: Manual of Remote Sensing 3rd edition Vol. 3, A. N. Rencz, Ed.

Clark, R.N., T.V.V. King, M. Klejwa, and G. A. Swayze, (1990). High Spectral Resolution Reflectance Spectroscopy of Minerals, J. Geophysical Research, vol. 95, pp. 12653—12680.

Eberl, D. D., Whitney, G., & Khoury, H. (1978). Hydrothermal reactivity of smectite. American Mineralogist, 63(3-4), 401-409.

Frolova, J., Ladygin, V., Rychagov, S., and Zukhubaya, D. (2014). Effects of hydrothermal alterations on physical and mechanical properties of rocks in the Kuril–Kamchatka island arc. Engineering Geology, 183, 80-95.

Fulignati, P., Malfitano, G., & Sbrana, A. (1997). The Pantelleria caldera geothermal system: data from the hydrothermal minerals. Journal of Volcanology and Geothermal Research, 75(3-4), 251-270.

Geiger, C.A. (2004) An introduction to spectroscopic methods in the mineral sciences and geochemistry. Ch. 1 in EMU Notes in Mineralogy, Vol.6, A.Beran and E. Libowitzky, Eds.

Henley, R. W., & Ellis, A. J. (1983). Geothermal systems ancient and modern: a geochemical review. Earth-science reviews, 19(1), 1-50.

Hulen, J. B., Collister, J. W., Johnson, S. D., & Allis, R. (1997). Oil in the Dixie Valley and Kyle Hot Springs geothermal systems, Nevada-Potentially sensitive indicators of natural and induced reservoir processes. In Twenty-fourth Workshop on Geothermal Reservoir Engineering, Stanford University, Caifornia.

Hulen, J. B., & Lutz, S. J. (1999). Altered volcanic rocks as hydrologic seals on the geothermal system of Medicine Lake volcano, California. Geothermal Resources Council Bulletin, 28(7), 217-222.

Huntington, J. F., Mauger, A. J., Skirrow, R. G., Bastrakov, E. N., Connor, P., Mason, P., ... & Whitbourn, L. B. (2006). Automated mineralogical core logging at the Emmie Bluff iron oxide-copper-gold prospect. MESA Journal, 41, 38-44.

Jones, C.G., and Moore, J.N., (2013). Petrographic and X-ray Diffraction Study of 4 Wells from Naval Air Station Fallon, Churchill County, Nevada: Report for the Navy Geothermal Program Office, Contract Number N62473_13_M_1404.

Kokaly, R. F., Graham, G. E., Hoefen, T. M., Kelley, K. D., Johnson, M. R., Hubbard, B. E., ... & Prakash, (2017) A. Multiscale Hyperspectral Imaging of the Orange Hill Porphyry Copper Deposit, Alaska, USA, with Laboratory-, Field-, and Aircraft-based Imaging Spectrometers. Conference Paper October 2017, Spectral Geology and Remote Sensing, Paper 84.

Mehmani, Y., Burnham, A. K., Berg, M. D. V., & Tchelepi, H. A. (2017). Quantification of organic content in shales via near-infrared imaging: Green River Formation. Fuel, 208, 337-352.

Patrier, P., Papapanagiotou, P., Beaufort, D., Traineau, H., Bril, H., & Rojas, J. (1996). Role of permeability versus temperature in the distribution of the fine (< 0.2 μm) clay fraction in the Chipilapa geothermal system (El Salvador, Central America). Journal of Volcanology and Geothermal research, 72(1-2), 101-120.

Reyes, A.G., (1990). Petrology of Philippine geothermal systems and the application of alteration mineralogy to their assessment. J. Volcanol. Geotherm Res., 43: 279-309.

Siler, D. L., Hinz, N. H., Faulds, J. E., Tobin, B., Blake, K., Tiedeman, A., ... & Rhodes, G. (2016). The geologic framework of the Fallon FORGE site. Geothermal Resources Council Transactions, 40, 573-584.

Siler, D. L., Hinz, N. H., Faulds, J. E., Ayling, B., Blake, K., Tiedeman, A., Sabin, A., Blankenship, D., Kennedy, M., Rhodes, G., Sophy, M. J., Glen, J. M.G., Phelps, G. A., Fortuna, M., Queen, J., Witter, J. (2018). The Geologic and Structural Framework of the Fallon FORGE site. PROCEEDINGS 43rd Workshop on Geothermal Reservoir Engineering, Stanford University, Feb 12-14, SGP-TR-213.

Thompson, A. J. (1999). Alteration mapping in exploration: Application of short wave infrared (SWIR) spectroscopy. Econ. Geol. Newsl., 30, 13.

Wyering, L. D., Villeneuve, M. C., Wallis, I. C., Siratovich, P. A., Kennedy, B. M., Gravley, D. M., & Cant, J. L. (2014). Mechanical and physical properties of hydrothermally altered rocks, Taupo Volcanic Zone, New Zealand. Journal of Volcanology and Geothermal Research, 288, 76-93.

Yagi, M., Yamada, Y., Okada, H., & Yamagishi, H. (2000, May). Occurrence and variation of clay minerals as hydrothermal scale in the Yamagawa geothermal wells, Kyusyu, Japan. In Proceedings world geothermal congress(Vol. 28).

Yang, K., J. F. Huntington, P. R. L. Browne, and C. Ma (2000), An infrared spectral reflectance study of hydrothermal alteration minerals from the Te Mihi sector of the Wairakei geothermal system, New Zealand, Geothermics, 29(3), 377-392.

Yang, K., P. R. L. Browne, J. F. Huntington, and J. L. Walshe (2001), Characterising the hydrothermal alteration of the Broadlands-Ohaaki geothermal system, New Zealand, using short-wave infrared spectroscopy, Journal of Volcanology and Geothermal Research, 106(1-2), 53-65.

Zhou, X., Jara, C., Bardoux, M., & Plasencia, C.(2017). Multi-Scale integrated application of Spectral Geology and Remote Sensing for Mineral Exploration. Conference Paper October 2017. Spectral Geology and Remote Sensing, Paper 82